Distribution Characteristics and Correlation of Edge Sharpness Threshold and Contact Area

Qian Wu and Jianguang Li

***Abstract*—It is currently unclear how sharpness discrimination ability is distributed across a wide range of edge sharpness and the effect of contact area on haptic perception. We 3D printed triangular prisms with various edge sharpness and half-edge widths in the full-scale range and conducted 2AFC tasks to gain the haptic threshold distribution. Results show that the distribution curves of the sharpness threshold and its contact area have a similar inflection point at 115°, implying a boundary between medium-low and high stimuli. It is also found that Weber fractions in the medium stimulus range follow Weber's Law and are consistent with previous studies but lower than the mean of Weber fractions in the high stimulus range. Besides, there is no significant difference in upper and lower thresholds in the medium-low stimulus range but a significant difference in the high stimulus range with the higher upper threshold. Variations in contact area do not affect sharpness discrimination ability when the half-edge width exceeds 2 mm. However, decreasing the half-edge width from 2 mm to 1 mm significantly reduces haptic sensitivity. Our findings offer preliminary evidence contributing to understanding haptic perception in edge sharpness discrimination, encompassing the properties of objects and object-individual interfaces.**

***Index Terms*—Contact area distribution, edge sharpness discrimination, haptic perception, Weber fraction,.**

I. Introduction

As ONE of the main ways for human beings to feel things and explore the world, the sense of touch plays a vital role in human-computer interaction. With the emergence of new technologies and interactive platforms (such as haptic displays in VR [1], [2], wearable devices [3], [4], and new interfaces [5], [6]), the research on haptic sensation and its mechanism is enriching and deepening [7]. In psychophysics, threshold refers to the minimum level of stimulation required to produce a noticeable change in perception [8]. As an essential indicator to describe haptic sensitivity and perception changes, the haptic threshold is a primary research object in haptic mechanisms.

Prior studies in haptic mechanism demonstrated discrimination abilities differed from the spatial properties of real objects, such as curvature [9], [10], length [11], and volume [12]. Scholars also conducted a series of studies to test haptic discrimination ability in different conditions, such as indirect contact [13], [14], interactive region [15], [16], exploration strategy [17], [18], health status [19], [20], [21], and simulated stimuli [22], [23], [24]. These studies have enriched the methodology and content of experimental psychophysics, exploring human haptic sensitivity to different objects and the various underlying factors and mechanisms that influence haptic perception.

The study of edge sharpness is equally essential as the haptic spatial properties mentioned above, as it represents a salient object feature that provides information about the shape [25]. The perception, simulation, and interaction of haptic information from natural objects heavily rely on the ability to detect edges and distinguish their length, curvature, and angle [26], [27], [28]. When we define an edge as being formed by the juncture of two surfaces, a fundamental property of an edge is the angle at which these surfaces meet, which is similar to the psychological dimension of sharpness. Skinner et al. [29] obtained the thresholds and Weber fractions of 4 triangular prisms varying from sharpness, and the results closely followed Weber's Law. Compared to previously reported Weber fractions from other haptic manipulations, the discrimination ability was sufficiently sensitive to changes in edge sharpness. They also found that the threshold in the free exploration condition was lower than that in the single touch condition, indicating that the exploration strategy affects sensitivity to edge sharpness. Further, Kent et al. [30] demonstrated that under the free exploration condition to feel the sharpness of the edge, a proximal-distal movement results in substantially lower sharpness discrimination thresholds than a medial-lateral movement.

Compared with studies on the full-range distribution of visual, auditory, and gustatory discrimination [31], current studies on sharpness discrimination are limited in stimuli scope. Only a few typical edges were selected, which lacks an overview to fully explore the haptic discrimination of all possible edges. Besides, limited studies investigated the relationship between a wide range of edges and their corresponding contact area distributions. As the contact area influences the sensitivity of human perception of softness and curvature, establishing this geometric relationship can aid in designing desired object properties in interaction design or haptic simulation [32], [33].

To address the above gaps, this study focused on the distribution of thresholds and contact areas for edge sharpness stimuli across a full range of scales. Two experiments were conducted to study the distribution characteristics and correlation of the

Manuscript received 8 May 2023; revised 8 October 2023 and 30 November 2023; accepted 20 January 2024. Date of publication 25 January 2024; date of current version 19 September 2024. This work was supported by the Digital Manufacturing Technology Lab, Harbin Institute of Technology. This paper was recommended for publication by Associate Editor M. Bianchi. *(Corresponding author: Qian Wu.)*

This work involved human subjects or animals in its research. The authors confirm that all human/animal subject research procedures and protocols are exempt from review board approval.

The authors are with the School of Mechatronics Engineering, Harbin Institute of Technology, Harbin 150001, China (e-mail: wuqian57@hit.edu.cn; mejgli@hit.edu.cn).

Digital Object Identifier 10.1109/TOH.2024.3357751

sharpness threshold and its contact area, respectively. In Experiment I, we 3D printed 36 triangular prisms with sharpness ranging from 0° to 175° and conducted a series of two-alternative forced-choice (2AFC) tasks [34] to obtain the sharpness threshold. Our analysis of the raw data revealed an inflection point in the threshold distributions, causing a change in slope. We also compared the Weber fraction and upper/lower threshold based on the inflection point and explored the correlation and distribution characteristics between the edge sharpness threshold and contact area. In Experiment II, we analyzed the contact area distribution and examined the degree of different contact areas with the same sharpness affecting the discrimination ability. This experiment utilized the same method and experimental procedure as Experiment I, but the test shapes with different half-edge widths. The outcomes of this study can further the understanding of haptic mechanisms by providing data support and be applied to the design and evaluation of haptic displays.

II. Experiment I: Edge Sharpness Threshold Distribution

A. Design

The main independent variable in Experiment I was edge sharpness, while the dependent variables included threshold and Weber fraction. Thirty-six triangular prisms featuring various angles and identical bases were fabricated by 3D printing to serve as test shapes. The participants touched the edges of these test shapes as sharpness stimuli. For the 3D printing, we utilized the Mono X 3D printer (Photon Mono X 4 K, Anycubic, China) with white resin. This printer boasts a 4 K LCD screen resolution, and the printing direction was aligned parallel to the edge, minimizing the impact of layer thickness on edge accuracy to ensure optimal shape precision and surface quality. The internal angle between two upper surfaces of each prism, denoted as angle θ, was changed from 5° to 180° with fixed increments of 5°.

Similar triangular prisms were employed in a previous study focusing on sharpness [29], and they introduced a variable denoted as S to streamline data analysis. This process was made because as sharpness perception increases, the internal angle θ decreases, which can complicate comparing results with other studies where stimulus measure increases with enhanced perception. In this study, the relationship between θ and S is defined as follows:

$$S = 180 - \theta \tag{1}$$

The range of sharpness S was varied from 0° to 175°. Edges with sharpness S exceeding 175° were not generated due to insufficient wall thickness for successful 3D printing. The surfaces of all test shapes were meticulously polished using 1000-grit sandpaper, resulting in uniformly smooth surfaces devoid of noticeable textures or defects. The bottom dimensions (30 mm × 20 mm) and height (20 mm from bottom to the edge) of all shapes remained consistent to control variables (Fig. 1). A fixed stand was used to ensure the test shapes maintained a relatively constant position throughout the experiment and predefined the initial finger touch position by baffles.

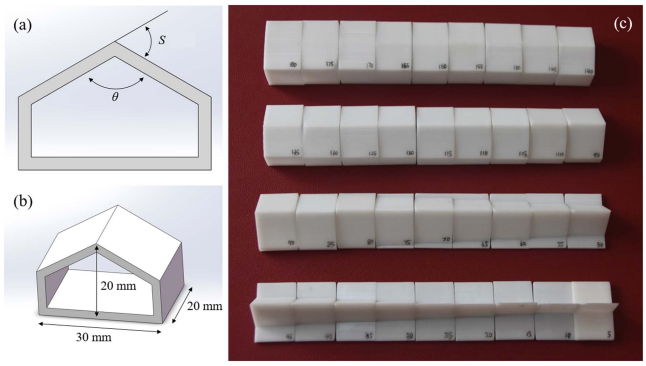

Fig. 1. Test shape (a) defines the internal angle θ and sharpness S, (b) illustrates dimensions and fabrication axes, and (c) shows the top view of 36 shapes.

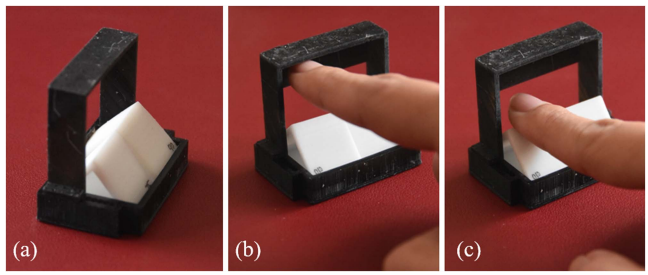

Fig. 2. Fixed stand (a) where 2 shapes were arranged side by side, (b) and (c) show one single press in the experiment.

B. Participants

Eleven participants were recruited for the study (3 identified as female, 8 as male) with ages ranging from 22 to 32 years (M = 26.91, SD = 2.64). All participants confirmed that they had not encountered any cognitive or sensory impairments that could hinder their capacity to comply with the experimental protocol. According to the Edinburgh Handedness Inventory [35], all participants were classified as right-handed. They possessed no prior knowledge of the research objective and had not participated in any other investigations regarding sharpness discrimination. Participants were compensated equally for their time.

C. Procedure

The 2AFC tasks were conducted to collect experimental data. The participant should cover his eyes and wear soundproof headphones to eliminate environmental influences on their haptic perception. The experimenter could give instructions to the participant through the earphone. During each trial, the participant touched two edges with varying sharpness, respectively, one as the reference and the other as the comparison. The shapes were arranged side by side on a fixed stand, ensuring consistency in their relative position to the participant (Fig. 2). The fixed stand was used to control the finger's initial position, press angle, and touch location and ensure the participant pressed vertically on the edge with identical movement stroke. The participant was instructed to touch the edge using one single press by the pad of his dominant index finger. The process began from

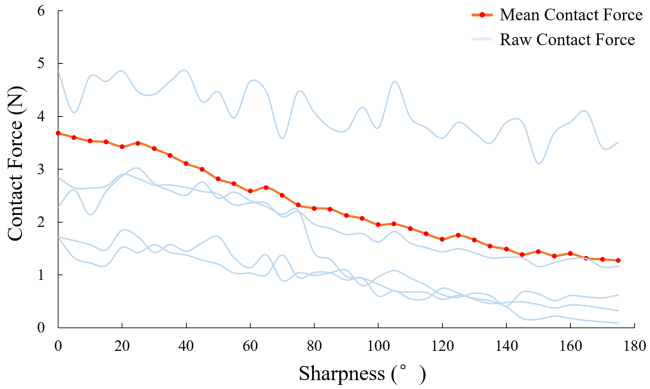

Fig. 3. Measured contact force in the pilot study from 5 participants. The red line indicates the mean contact force.

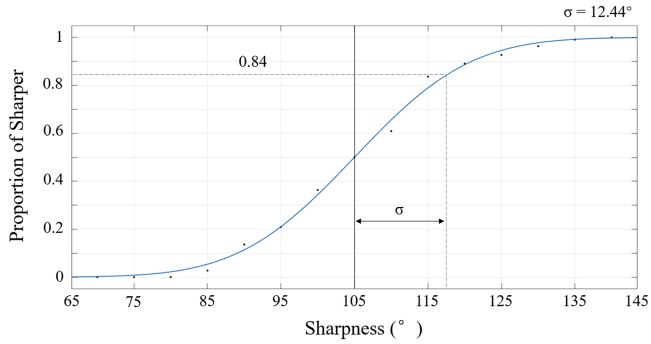

Fig. 4. Example of data collected. The curve shows the fitted function through the measured data points. The vertical line at 105° indicates the sharpness of the reference shape. The dashed line specifies the place of the 84% threshold. The value of this discrimination threshold, σ, is shown in the top right corner of the figure.

the fixed stand's upper and left baffles, then touched down at the approximate midpoint of the shape's edge. The participant remained still without any relative movement until the haptic perception was completed, with a time limit of 3 seconds. Subsequently, the participant lifted his finger, moved it to the upper and right baffles, and completed the second single press. The participant should always first touch the left edge and then the right edge, and be asked to report which edge (left or right) feels sharper. Between trials, the participant placed his right hand on the marked location in front of the fixed stand to reset the position and then had a break.

We conducted a pilot study involving five participants to measure the contact force during a single press on all edges using an electronic scale ranging from 0 to 1 kg. The results indicated a decrease in contact force as sharpness increased (see Fig. 3). Subsequently, participants were asked to compare edges with reference angles of 160°, 120°, 90°, 60°, and 30°, following the experimental procedure. They were instructed to adjust their contact force to match the mean contact force for each edge (the red line in Fig. 3). Experimenters reminded participants to ensure that the change in contact forces remained within a 30 g range from the mean. Following this pilot study, two participants reported discomfort while touching 60° and 30° edges using the mean contact force. One participant mentioned difficulty perceiving the edge when adhering to the mean contact force. Additionally, four participants reported that focusing on controlling the contact force hampered their ability to concentrate on comparing the edges, resulting in longer exploration time. According to the pilot study results and related research that did not control the contact force [29], [30], the contact force in Experiment I was not controlled.

For each reference shape, 14 comparison shapes (if available) were used with 7 higher sharpness and 7 lower sharpness relative to the reference. The difference in sharpness between the comparison shapes and the reference shape ranged from 5° to 35°, with sharpness increments of 5°. During the experiment, each pair of reference and comparison shapes was presented ten times, with positions balanced (five times on the left and five times on the right), resulting in 2240 presentations. The order of the stimuli was randomized throughout the experiment. To avoid fatigue and pressure pain from prolonged touch acuity, the experiment was divided into several 15-minute blocks, each comprising approximately 70 continuous trials, with at least 5 minutes of rest between blocks. Participants were limited to conducting six blocks daily, with a maximum of three consecutive blocks. It took about 8–9 hours to complete the entire experiment.

D. Analysis

To accurately calculate the proportion of the correct identification of the sharper edge for each combination of reference and comparison shapes in the original data set, a weighted cumulative Gaussian distribution (f) was used as a function of the sharpness of edges (S). The data were fitted using a maximum-likelihood procedure [36], which followed the equation below:

$$f(S) = \frac{1}{2}\left[1 + erf\left(\frac{S - S_{ref}}{\sigma\sqrt{2}}\right)\right] \tag{2}$$

where $erf()$ represents the Gauss error function, and the parameter σ reflects the participant's sensitivity to detect differences in sharpness between two shapes, corresponding to the perceptual threshold of the reference edge (Fig. 4). The parameter S_{ref} represents the sharpness of the reference edge. Based on Weber's Law, the Weber fraction k is obtained by the following equation:

$$k = \frac{\sigma}{S_{ref}} \tag{3}$$

The distribution curve is plotted using the calculated sharpness threshold. According to Weber's Law, the Weber fraction is expected to remain constant within the medium stimulus range, while the Weber fraction in the low and high stimulus ranges may change depending on the stimuli. Two inflection points representing the endpoints of the medium stimulus range divide the distribution curve of the Weber fraction into three parts, and (4) is used for the curve estimation. Based on (3), the Weber fraction can be expressed as the slope of the threshold distribution, thus rendering the threshold distribution as a linear function within the medium stimulus range. By observing the curve, the slope of the curve changes at a certain inflection point,

which can be located using a segmented fitting method using (5).

$$f_w(S) = \begin{cases} G(S), & \text{if } S < S_{i1} \\ k_0, & \text{if } S_{i1} \le S \le S_{i2} \\ G(S), & \text{if } S > S_{i2} \end{cases} \quad (4)$$

$$f_t(S) = \begin{cases} a_0 S + a_1, & \text{if } S \le S_{i2} \\ G(S), & \text{if } S > S_{i2} \end{cases} \quad (5)$$

where k_0 is the estimated Weber fraction by segmented fitting. S_{i1} and S_{i2} are the sharpness of the theoretical inflection points obtained by one-sample Wilcoxon signed rank test on the Weber fractions in Experiment I. a_0 and a_1 are the parameters related to the linear function. *G(S)* represents the set of fitting equations (see Equation (6)–(12)) including the linear, inverse, quadratic, cubic, power, S-curve, and exponential models [37]. We changed *G(S)* in every fitting process to obtain the best fitting parameters. *G(S)* ($S < S_{i1}$) and *G(S)* ($S > S_{i2}$) could be different. The segmented fitting model will output a R^2 that represents the fitting quality of the curve.

$$Linear: G(S) = b_0 + b_1 S \quad (6)$$

$$Inverse: G(S) = b_0 + \frac{b_1}{S} \quad (7)$$

$$Quadratic: G(S) = b_0 + b_1 S + b_2 S^2 \quad (8)$$

$$Cubic: G(S) = b_0 + b_1 S + b_2 S^2 + b_3 S^3 \quad (9)$$

$$Power: G(S) = b_0 S^{b_1} \quad (10)$$

$$S-curve: G(S) = exp\left(b_0 + \frac{b_1}{S}\right) \quad (11)$$

$$Exponential: G(S) = b_0 exp(b_1 S) \quad (12)$$

E. Results

Due to Weber fractions of the reference shapes not following a normal distribution (p-values of the Shapiro-Wilk test were less than 0.05), a one-sample Wilcoxon signed rank test on the Weber fractions was conducted to test the disparity to the Weber fraction of 0.11 provided by Skinner's research [29] and determine S_{i1} and S_{i2}. Data at 0° were excluded due to the absence of Weber fraction values. The results are presented in Table I. It indicates that the discrepancy between the medians of Weber fractions in [35, 115] and the Weber fraction from the previous study as 0.11 is not statistically significant, while the medians of Weber fractions in other ranges are significantly higher than 0.11.

We used *G(S)* as the curve estimation model and segmented fitting model through (4) to analyze the Weber fraction distribution curve (the red line in Fig. 5) with S_{i1} as 35° and S_{i2} as 115°. The curve estimation results are shown in Table II. The definition of R^2 states that, as the Corrected Sum of Squares is constant for one set of data, the smaller the Residual Sum of Squares (RSS) is, the larger the R^2 is. Although there is a same best R^2 of 0.985 when *G(S)* ($S < S_{i1}$) is the inverse model and *G(S)* ($S > S_{i2}$) is the quadratic or cubic model, the best-fit function use the cubic model as *G(S)* ($S > S_{i2}$) with the lowest RSS of 0.00777. Where $k_0 = 0.113 \pm 0.000$, the parameters of *G(S)* ($S < S_{i1}$) are: $b_0 = -0.077 \pm 0.000$, $b_1 = 3.719 \pm 0.000$, and the parameters of *G(S)* ($S > S_{i2}$) are: $b_0 = 0.327 \pm 0.001$, $b_1 = -0.009 \pm 0.123$, $b_2 = 7.848{*}10^{-5} \pm 0.083$, $b_3 = -2.049{*}10^{-7} \pm 0.004$. The threshold distribution curve (the blue line in Fig. 5) was also analyzed through curve estimation. The best segmented fitting is (5) with *G(S)* as the cubic model ($R^2 = 0.958$), which also indicates the same inflection point of 115°. The parameters of the function are: $a_0 = 0.087 \pm 0.013$, $a_1 = 2.28 \pm 0.861$, $b_0 = 36.048 \pm 508.96$, $b_1 = -0.953 \pm 10.494$, $b_2 = 0.01 \pm 0.072$, $b_3 = -2.399{*}10^{-5} \pm 0.000$. The results of curve estimation using *G(S)* were compared with the result of segmented fitting, where the exponential model has the best fitting accuracy ($R^2 = 0.967$), with $b_0 = 0.014 \pm 0.000$ and $b_1 = 3.107 \pm 0.139$.

Weber's Law stipulates that Weber fractions should remain constant in the medium stimulus range. However, Table I and the red distribution curve in Fig. 5 indicate that the Weber fraction in (0, 35) does not follow this trend. Some previous works established that Weber's Law is inapplicable in the low stimulus range [31], [38]. Therefore, the data in this range will not be analyzed based on Weber's Law. According to the results of the

TABLE I
RESULTS OF ONE-SAMPLE WILCOXON SIGNED RANK TEST ON WEBER FRACTIONS IN [5, 175]

Sharpness(°)	Median	P-value	Sig.
5	0.779	0.003	**
10	0.389	0.003	**
15	0.314	0.003	**
20	0.194	0.003	**
25	0.219	0.003	**
30	0.157	0.007	**
35	0.116	0.182	
40	0.127	0.13	
45	0.122	0.01	**
50	0.133	0.593	
55	0.01	0.248	
60	0.091	0.075	
65	0.094	0.374	
70	0.097	0.182	
75	0.114	0.373	
80	0.102	0.091	
85	0.091	0.021	*
90	0.138	0.075	
95	0.118	0.033	*
100	0.138	0.12	
105	0.103	0.79	
110	0.117	0.722	
115	0.125	0.328	
120	0.145	0.006	**
125	0.159	0.016	*
130	0.137	0.01	**
135	0.14	0.003	**
140	0.157	0.008	**
145	0.207	0.004	**
150	0.19	0.004	**
155	0.175	0.003	**
160	0.13	0.01	**
165	0.151	0.004	**
170	0.165	0.01	**
175	0.185	0.004	**

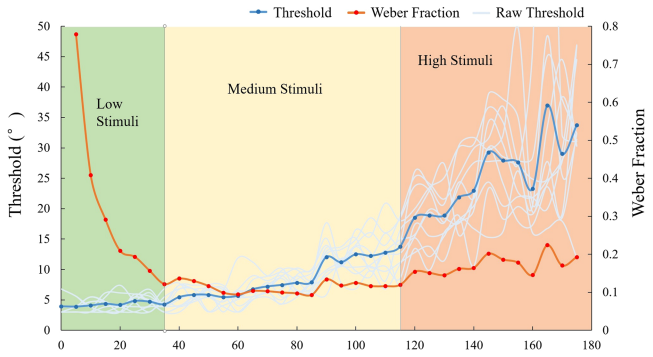

Fig. 5. Distributions of Weber fraction and threshold, where can be divided into 3 ranges with different stimulation intensities according to Weber's Law and the inflection points of the threshold.

TABLE II
CURVE ESTIMATION RESULTS OF THE WEBER FRACTION DISTRIBUTION IN [5, 175] WITH $S_{i1} = 35°$ AND $S_{i2} = 115°$

Curve Estimation	$G(S)$ $(S < S_{i1})$	$G(S)$ $(S > S_{i2})$	R^2	RSS
Linear			0.091	0.463
Inverse			0.854	0.074
Quadratic			0.526	0.241
Cubic			0.769	0.118
Power			0.29	4.546
S-curve			0.628	2.384
Exponential			0.03	6.213
Segmented fitting	Inverse	Linear	0.984	0.008
Segmented fitting	Inverse	Inverse	0.984	0.008
Segmented fitting	Inverse	Quadratic	0.985	0.00778
Segmented fitting	Inverse	Cubic	0.985	0.00777
Segmented fitting	Inverse	Power	0.984	0.008
Segmented fitting	Inverse	S-curve	0.984	0.008
Segmented fitting	Inverse	Exponential	0.984	0.008
Segmented fitting	Quadratic	Cubic	0.965	0.018
Segmented fitting	Cubic	Cubic	0.983	0.009
Segmented fitting	S-curve	Cubic	0.962	0.019

Wilcoxon signed rank test on Weber fractions and segmented fitting, the data in [35, 175] was divided into two parts: [35, 115] and (115, 175], and an independent sample t-test was conducted between them to compare the difference. The data is normally distributed with no outliers. The independent sample t-test shows that the mean value of Weber fraction in (115, 175] (M = 0.173, SD = 0.024) is significantly higher (t = −7.649, p = 0.000) than that in [35, 115] (M = 0.113, SD = 0.014), with a difference of 0.051 (95% CI: −0.076 to −0.043).

Because the overlarge (small) sharpness edges have insufficient fitting points to calculate the lower (upper) threshold, not all shapes could be used to accurately calculate upper and lower thresholds in the sharpness range [0, 175]. For instance, an edge with 0° sharpness only has an upper threshold but no lower threshold. To ensure the reliability of experimental data, the sharpness range [20, 150] was chosen due to at least 5 fitting data points of upper or lower thresholds.

We conducted a one-sample Wilcoxon signed rank test on the Weber fractions of the upper threshold (DLU) and lower threshold (DLD) to test their disparity to the previous result of 0.11, and the results are shown in Table III. There are no significant differences between most Weber fractions of DLU and DLD in [35,115], while the medians in other ranges are significantly higher than 0.11. The results of the segmented fitting (Fig. 6) using (5) indicate that when S_{i2} is 115°, it has best fitting accuracy for the upper threshold ($R^2 = 0.91$) and the lower threshold ($R^2 = 0.924$) while $G(S)$ as the cubic model

TABLE III
RESULTS OF ONE-SAMPLE WILCOXON SIGNED RANK TEST ON WEBER FRACTIONS OF DLU AND DLD IN [20, 150]

Sharpness(°)	Weber Fraction of DLU			Weber Fraction of DLD		
	Median	P-value	Sig.	Median	P-value	Sig.
20	0.194	0.002	**	0.194	0.003	**
25	0.272	0.003	**	0.155	0.002	**
30	0.13	0.105		0.227	0.006	**
35	0.111	0.108		0.111	0.857	
40	0.108	0.285		0.097	0.422	
45	0.151	0.15		0.086	0.592	
50	0.123	1		0.136	0.239	
55	0.1	0.324		0.079	0.368	
60	0.091	0.371		0.091	0.212	
65	0.127	0.026	*	0.06	0.049	*
70	0.097	0.248		0.097	0.789	
75	0.073	0.109		0.091	0.929	
80	0.13	0.373		0.068	0.006	**
85	0.087	0.041	*	0.095	0.02	*
90	0.187	0.01	**	0.068	0.021	*
95	0.114	0.929		0.121	0.286	
100	0.146	0.01	**	0.106	0.656	
105	0.118	0.374		0.113	0.929	
110	0.087	0.534		0.126	0.062	
115	0.162	0.026	*	0.083	0.026	*
120	0.216	0.003	**	0.087	0.131	
125	0.216	0.026	*	0.117	0.026	*
130	0.139	0.075		0.148	0.013	*
135	0.205	0.003	**	0.088	0.155	
140	0.153	0.01	**	0.156	0.016	*
145	0.279	0.003	**	0.142	0.013	*
150	0.205	0.033	**	0.19	0.003	**

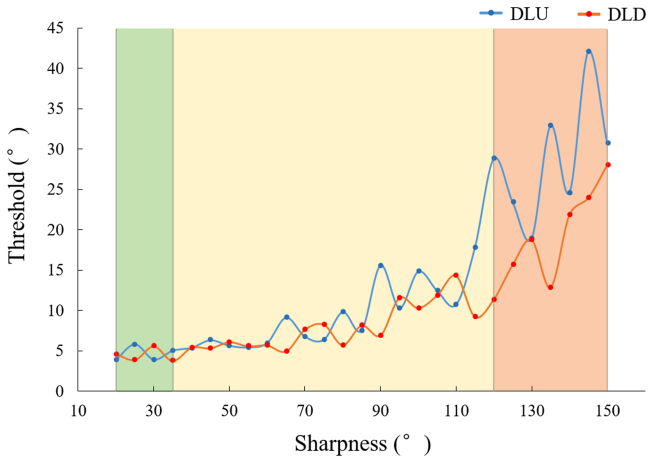

Fig. 6. Distributions of the upper threshold (DLU) in the blue line and lower threshold (DLD) in the red line, and the infection point is 115°.

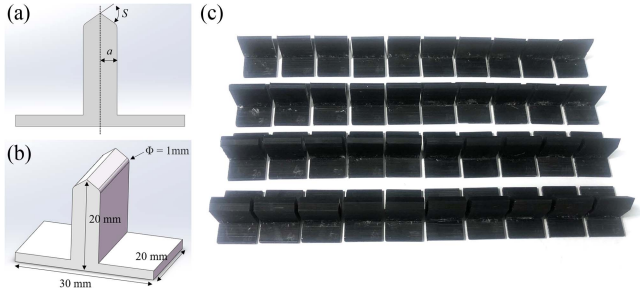

Fig. 7. Test shape (a) defines the sharpness S and half-edge width a, (b) illustrates with dimensions and fabrication axes, (c) shows the top view of 40 shapes.

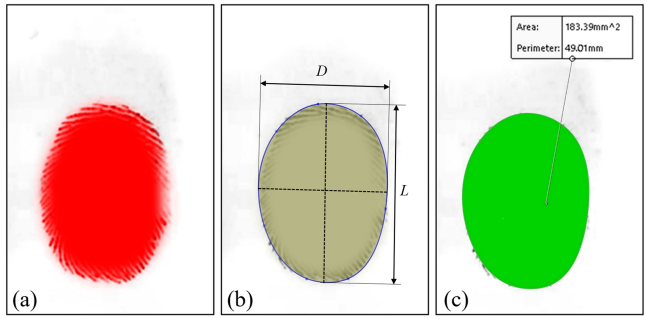

Fig. 8. Fingerprints and contact area analysis. (a) Fingerprints stamped onto the paper and scanned into. jpg format at the original scale. (b) The outer contour, contact width and length were marked by the researchers. (c) The contact area output from the software. The fingerprint in this figure has been partially obscured to protect participant privacy.

(see (9)). The parameters of the segmented function for DLU are: $a_0 = 0.12 \pm 0.029$, $a_1 = 3.275 \pm 1.536$, $b_0 = 12448.545 \pm 4625.529$, b_1 = -276.19 $\pm$ 103.351, $b_2 = 2.038 \pm 0.768$, $b_3 = -0.005 \pm 0.002$; for DLD are: $a_0 = 0.088 \pm 0.017$, $a_1 = 3.446 \pm 0.882$, b_0 = -2688.982 $\pm$ 2656.128, $b_1 = 61.088 \pm 59.348$, $b_2 = -0.462 \pm 0.441$, $b_3 = 0.001 \pm 0.001$. The data is divided into two parts: [20, 115] and (115, 150], and their upper and lower thresholds are further compared.

The data in [20, 115] and (115, 160] conform to the normal distribution (p-values of the Shapiro-Wilk test were higher than 0.05) without outliers, so we conducted a paired sample t-test to compare the difference between DLU and DLD in each range. The results show that there is no significant difference ($t = 1.613$, $p = 0.123$) between the upper ($M = 8.44$, $SD = 4.05$) and lower ($M = 7.256$, $SD = 2.905$) threshold distributions in [20, 115]. In contrast, the mean value of the upper threshold ($M = 28.789$, $SD = 7.548$) was significantly higher ($t = 3.076$, $p = 0.022$) than that of the lower threshold ($M = 18.946$, $SD = 6.063$) in (115, 150]. The difference was 9.843° (95%CI: 2.012° to 17.674°).

III. Experiment II: Correlation of Sharpness Discrimination and Contact Area

The results of Experiment I reveal the presence of an inflection point within the sharpness threshold distribution. Significant differences exist in the sharpness discrimination ability and the upper and lower thresholds on both sides of the inflection point. We designed and conducted Experiment II to explore the potential influence of variations in contact area on these results.

A. Design

The main independent variable of Experiment II was the contact area, and the dependent variable was the Weber fraction. In this study, the contact area represents 'the gross area' corresponding to the overall area comprising the elliptical shape encompassing the entire contact [39]. We fabricated four sets of triangular prisms with various sharpness and half-edge widths as test shapes, which are shown in Fig. 7. The 3D printer, materials (excluding the color), and parameters used in Experiment II were consistent with those in Experiment I. The range of sharpness S was varied from 30° to 120° with increments of 10°. The half-edge width a differed among the four sets and was measured as 4 mm, 3 mm, 2 mm, and 1 mm, respectively. Additionally, we employed Weber fractions to analyze the data collectively from Experiments I and II.

B. Participants

The participants involved in Experiment II were the same as those in Experiment I.

C. Procedure

Before Experiment II, we employed the imprint method, as described by Hauser et al. [40], to measure the contact area between the finger and various edges used in Experiment I under identical touching conditions. In this procedure, participants coated their testing fingers with washable red ink and single pressed all edges. The surface of the edges was covered with sulfuric acid paper to record the contact area during pressing. Subsequently, the fingerprints were scanned into the computer as image files, preserving their original scale. Researchers then utilized image processing software (Adobe Photoshop and Solidworks) to manually outline the outer contours and calculate the corresponding contact areas. Additionally, we measured the contact length L (the longest median perpendicular to the edge) and width D (the longest median parallel to the edge), as shown in Fig. 8.

2AFC tasks were conducted to collect the data in Experiment II, and participants were asked to single press the edge in every trial. The procedures closely mirrored those implemented in Experiment I. We measured sharpness thresholds at 50°, 70°, and 90° from the medium stimulus range, selected based on earlier study [29] involving half-edge widths of approximately 4 mm. For the sharpness of 50°, we used the sharpness of 30°, 40°, 60°, and 70° as the comparison shapes; For the sharpness of 70°, we used the sharpness of 50°, 60°, 80°, and 90° as the comparison shapes; For the sharpness of 90°, we used the sharpness of 70°, 80°, 100°, 110°, and 120° as the comparison shapes. During the experiment, each pair of reference and comparison shapes was presented 10 times, with positions balanced (5 times on the left and 5 times on the right), for a total of 520 presentations. The order of presentation remained randomized throughout the experiment, and it took about 2 hours.

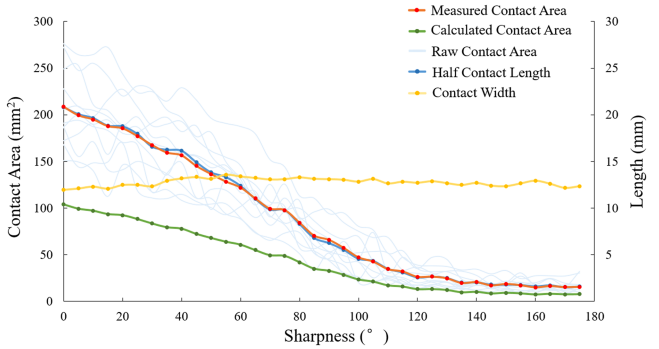

Fig. 9. Distributions of raw, calculated, and measured contact area, half-contact length, and contact width for full range of sharpness.

D. Analysis

The calculation process of the threshold and Weber fraction and the segmented fitting method for the distribution curve of the contact area are similar to Experiment I, where using the following equation:

$$f_c(S) = \begin{cases} G(S), & \text{if } S \le S_{i2} \\ G(S), & \text{if } S > S_{i2} \end{cases} \tag{13}$$

An elliptical shape was assumed to estimate the contact area, where the semi-major and semi-minor axes corresponded to half of the contact length and width, respectively. The area of the ellipse was calculated using (14), with A representing the area of the ellipse, L and D denoting the contact length and width, and l indicating half of the contact length:

$$A = \frac{1}{4}\pi LD = \frac{1}{2}\pi lD \tag{14}$$

The contact width remained consistent (the yellow line in Fig. 9) across various sharpness for each participant (M = 12.779, SD = 0.411). This is supported by the calculated contact area using (14), which closely aligns with the measured contact area. The contact length exhibited variation with changing sharpness. Distribution curves for the half-contact length, contact area calculated using (14), and measured contact area were plotted (shown in Fig. 9). These three curves are almost identical, which indicates that the half-contact length can replace the contact area as the independent variable in Experiment II. This substitution is advantageous because controlling the contact area is challenging. The half-contact length can be calculated using the half-edge width a and sharpness S with the following equation:

$$l = \frac{a}{\sin\left(90 - \frac{S}{2}\right)} \tag{15}$$

E. Result

Curve estimation and segmented fitting were used to estimate the distribution curve of the contact area, and results are shown in Table IV. According to the results, the infection point with the highest fitting accuracy ($R^2 = 0.998$) is 115°, and the fitting model is (13) with both the *G(S)* ($S \le S_{i2}$) and *G(S)* ($S > S_{i2}$) is the cubic model. The result is similar to the segmented fitting of the threshold distribution curve. The parameters of *G(S)* ($S \le S_{i2}$) are: $b_0 = 204.38 \pm 0.000$, $b_1 = -0.532 \pm 0.003$, $b_2 = -0.021 \pm 705.066$, $b_3 = 0.0001 \pm 0.099$. The parameters of *G(S)* ($S > S_{i2}$) are: $b_0 = 42.162 \pm 2.122$, $b_1 = 0.557 \pm 0.000$, $b_2 = -0.009 \pm 14.538$, $b_3 = 3.014{*}10^{-5} \pm 0.163$.

TABLE IV
CURVE ESTIMATION RESULTS OF THE CONTACT AREA DISTRIBUTION IN [0, 175] WITH $S_{i2} = 115°$

Curve Estimation	*G(S)* ($S \le S_{i2}$)	*G(S)* ($S > S_{i2}$)	R^2	RSS
Linear			0.938	10044.856
Quadratic			0.982	2920.638
Cubic			0.996	707.055
Exponential			0.969	0.966
Segmented fitting	Linear	Linear	0.995	708.217
Segmented fitting	Linear	Quadratic	0.996	699.982
Segmented fitting	Linear	Cubic	0.996	699.803
Segmented fitting	Linear	Exponential	0.996	707.251
Segmented fitting	Quadratic	Cubic	0.997	531.88
Segmented fitting	Cubic	Cubic	0.998	245.326
Segmented fitting	Exponential	Cubic	0.968	5256.362

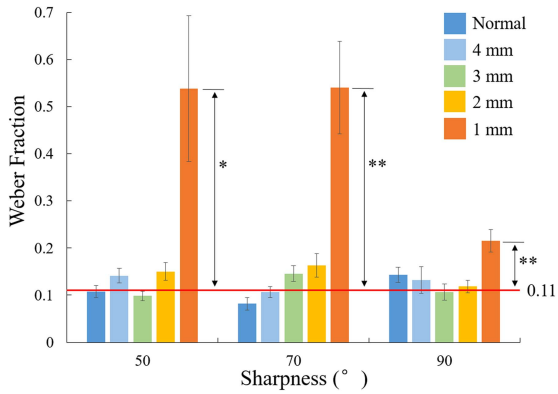

Fig. 10. Weber fractions of edged with different sharpness (50°, 70°, and 90°) and half-edge widths (4 mm, 3 mm, 2 mm, and 1 mm), and the red line indicates the mean Weber fraction of sharpness as 0.11. The blue box named normal indicates the Weber fractions in Experiment I.

The Weber fraction is shown in Fig. 10. One-sample t-tests were used to compare the data to the results of Skinner's research [29]. There are no significant differences between the mean Weber fractions of 50°, 70°, and 90° with the half-edge width as 4 mm, 3 mm, and 2 mm and the mean Weber fraction in the medium stimulus range as 0.11. By contrast, the mean Weber fractions of 50° (M = 0.538, SD = 0.514, t = 2.762, p = 0.02), 70° (M = 0.54, SD = 0.325, t = 4.388, p = 0.001) and 90° (M = 0.215, SD = 0.079, t = 4.433, p = 0.001) with the half-edge width as 1 mm are significantly higher than 0.11. Based on (15), the half-edge width at 1 mm and 2 mm corresponds to the half-contact length at 1.246 mm and 2.492 mm. The half-contact length of the inflection point at 115° is 1.599 mm, between 1.246–2.492 mm. Fig. 11 shows the distribution of the half-contact length in Experiment II.

IV. DISCUSSION

The distribution analysis results reveal an inflection point in the distribution curves of contact area and perception threshold

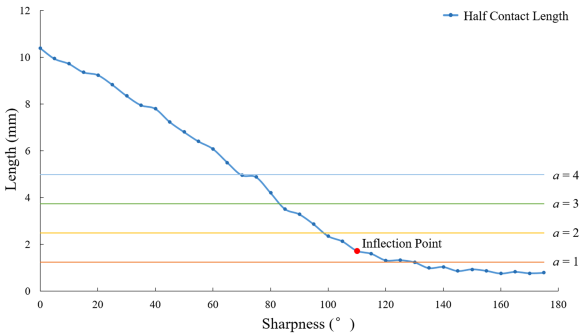

Fig. 11. Distribution of the half-contact length for the full range of sharpness. The constant lines indicate the corresponding half-contact length of the half-edge widths used in Experiment II, and the red spot shows the location of the inflection point.

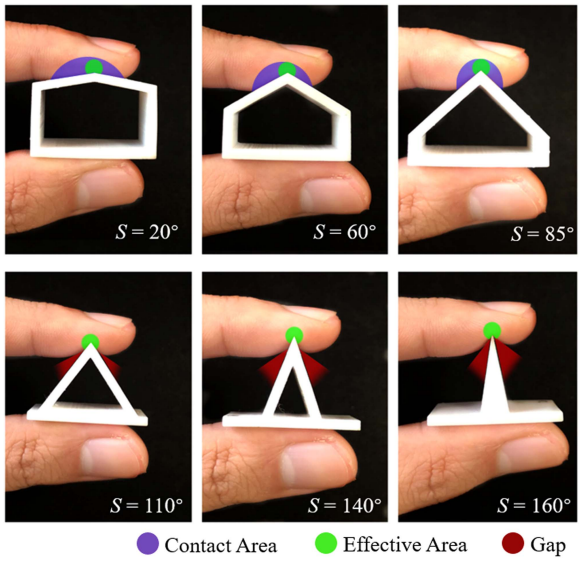

Fig. 12. Side views of the finger press on the edge of the shapes vary in sharpness. A gap occurs when the fingers cannot fit the edge, and the contact area at this point is similar to the effective contact area.

at 115°. This inflection point divides the distribution curves into two parts: one in the preceding range [0, 115] and another in the subsequent range (115, 175], each characterized by different slopes. In the [0, 115] range, the contact area distribution curve exhibits a more pronounced rate of change than that in the (115, 175] range. Conversely, the threshold distribution curve in the [0, 115] range displays a lower change rate than the (115, 175] range. This abrupt shift in the contact area distribution can be attributed to both the finger's elasticity and interaction depth limitations. Fig. 12 provides a side view of the interaction between the fingerpad and edges with various sharpness. At lower sharpness (20°, 60°, and 85°), the finger can conform closely to the edge, where the contact area is primarily based on the length of contact and the maximum interaction depth between the finger and the edge, leading to a substantial rate of change in the contact area. In contrast, at higher sharpness (110°, 140°, and 160°), the finger and the edge cannot fit well due to the elastic limit of the finger, leading to a more modest change in the contact area.

The sudden mutation in the threshold, marked by a significant change in the slope, is closely associated with alterations in the contact area distribution. This change in the threshold distribution, quantified as the slope of the curve, serves as an alternative expression of human haptic discrimination ability. The similar changing trend between threshold change and the contact area aligns with prior research, as also reported by Goodwin [41]. Pont et al. [15] suggested that the maximum contact length of different hand areas is crucial in determining the threshold, not the specific contact area. The results verified Goodwin's study [33] that humans can discriminate spherically curved surfaces without recourse to the accompanying changes in the contact area. Once the contact area reaches a critical value (i.e. the effective contact area in Fig. 12), its alteration will not affect threshold change. In our study, when the contact area distribution comes to the inflection point, it may also meet the critical value required for sharpness perception. As the effective contact area diminishes, the number of mechanoreceptors also decreases, consequently diminishing haptic discrimination ability, as evidenced by a reduced rate of change in the threshold. However, any numerical decrease does not impact the threshold change rate when the contact area exceeds this critical value, which affirms Weber's Law.

To facilitate the discussion of our study results, we introduce two definitions: 'effective contact area' and 'ineffective contact area'. For the edges, the 'effective contact area' pertains to the region closely encircling the edge impression, while the 'ineffective contact area' comprises the area outside this region. Prior studies [42], [43] have suggested that haptic discrimination ability hinges on the number and activation level of mechanoreceptors in the skin of the fingers. We posit that only mechanoreceptors within the effective contact area are activated during touch. The extent of their activation corresponds to the strength of the stimulus, i.e., the depth to which the edge penetrates the finger. Based on the results of Experiment I, we categorize the sharpness range into three distinct ranges: the 'low stimulus range' ranging from [0, 35), the 'medium stimulus range' ranging from [35, 115], and the 'high stimulus range' ranging from (115, 175]. The inflection point at 115° in distributions of the threshold and the contact area demarcates the medium-low and high stimulus ranges.

In the low stimulus range, edge sharpness is relatively mild. As sharpness gradually intensifies, the depth to which the edge penetrates the finger increases, while the contact area gradually diminishes due to skin stretching. Results from Experiment I reveal a monotonic decrease in the Weber fraction within this range, indicating an augmentation in the finger's discrimination ability as stimulus strength increases. This phenomenon seems to be primarily associated with stimulus strength rather than the contact area. Although the number of mechanoreceptors in this zone remains constant, their activation level amplifies with the stimulus, resulting in an enhanced resolution ability. This enhancement manifests as a logarithmic curve, consistent with findings from Alfred's research [31].

In the medium stimulus range, the depth to which the edge penetrates the finger remains consistent as sharpness increases. The number and activation level of mechanoreceptors remain at their peak within the medium stimulus range, resulting in a constant discrimination ability consistent with Weber's Law. Conversely, the contact area decreases due to alterations in the ineffective contact area, signifying that variations in contact area do not impact discrimination ability in this range.

In the high stimulus range, the ineffective contact area has diminished to zero, and alterations in the contact area exclusively impact the effective contact area. While the activation level of the mechanoreceptors remains at its peak due to the maximum depth to which the edge penetrates the finger, the quantity of mechanoreceptors decreases in tandem with the decrease in the effective contact area, leading to a decrease in discrimination ability. Consequently, the Weber fraction significantly increases.

Remarkably, both upper and lower thresholds share a similar inflection point in their distribution, situated precisely at 115°. As expounded upon earlier, this inflection point differentiates between the medium-low and high stimulus ranges within the distributions of both upper and lower thresholds. The distinction between the distribution of the upper and lower thresholds is primarily marked by the inflection point, with the upper threshold exhibiting a significantly higher value than the lower threshold in the high stimulus range. The results of the paired sample t-test indicate no significant difference in the distribution of upper and lower thresholds within the medium-low stimulus range. However, the upper threshold is significantly higher than the lower threshold in the high stimulus range. These findings can be elucidated by considering the upper and lower thresholds' range. In the high stimulus range, the fitting points of the upper thresholds of stimulation points are all located in the high stimulus range, where discrimination ability is comparatively limited, leading to a high threshold value. In contrast, the lower threshold remains in the medium-low stimulus range, characterized by superior discrimination ability compared to the high stimulus range, resulting in a low threshold value.

Furthermore, the contact area at the intersection of the medium and high stimulus ranges can be regarded as the effective contact area, aligning with the inflection point of the distribution curve at 115°. We calculated the effective contact area at the inflection point to be 32.098 mm^2, with a corresponding half-contact length of 1.599 mm. Experiment II involving different half-edge widths at the same sharpness further validated this hypothesis. The Weber fractions were identical for half-edge widths greater than 2 mm (corresponding to the half-contact length of 2.492 mm), despite variations in the contact area, and exhibited no significant differences. However, for a half-edge width of 1 mm (corresponding to the half-contact length of 1.246 mm), the Weber fractions for different sharpness were significantly higher than in other cases. The corresponding half-contact length at the inflection point is within the range of 1.246–2.492 mm, consistent with the above calculations, indicating a maximum effective area.

V. Conclusion, Limitation and Future Work

In this study, we investigated the distribution characteristics of the haptic threshold and its contact areas across the full range of edge sharpness, and explored the potential correlation between changes in contact area and sharpness discrimination ability. We discovered a consistent inflection point at 115° in the distribution curves of both the contact area and the sharpness threshold, then analyzed the differences and characteristics in the distribution on both sides of the inflection point. Our results reveal that this inflection point in the threshold distribution separates the medium-low and high stimulus ranges. Within the medium stimulus range, the Weber fraction distribution follows Weber's Law, the results of previous studies. Furthermore, the difference in the distribution of the upper and lower thresholds is distinguished by this inflection point, where the upper threshold is significantly higher than the lower threshold in high stimulus ranges. Only when the contact area is smaller than the effective contact area, does the change in the contact area affect the discrimination ability. The outcomes of this study provide valuable insights for understanding the mechanisms of haptic perception and can be applied to inform the design of resolution and user studies in haptic displays.

The limitation of this study was not controlling the contact force while measuring the contact area of the finger pressing on the edge. Although passive touch by mechanically pressing is easy to control the contact force, active touch aligns more closely with individuals' habitual actions during real interactions than passive touch. However, participants actively controlling the contact force during the touch process might cause distraction, potentially impacting haptic perception abilities. It is essential to provide reminders and assistance in controlling the contact force through the experimental setup and determine the contact force range for precise control.

Future research will investigate the distribution of other haptic stimuli, such as curvature and spheres, to determine whether similar correlations and distribution characteristics exist for their thresholds and contact areas. If such correlations exist, we aim to develop a method for predicting haptic thresholds and Weber fractions based on shape and contact area.

References

[1] A. F. Siu, E. J. Gonzalez, S. Yuan, J. B. Ginsberg, and S. Follmer, "Shapeshift: 2D spatial manipulation and self-actuation of tabletop shape displays for tangible and haptic interaction," in *Proc. CHI Conf. Hum. Factors Comput. Syst.*, 2018, pp. 1–13.

[2] S. V. Salazar, C. Pacchierotti, X. de Tinguy, A. Maciel, and M. Marchal, "Altering the stiffness, friction, and shape perception of tangible objects in virtual reality using wearable haptics," *IEEE Trans. Haptics*, vol. 13, no. 1, pp. 167–174, Jan.-Mar. 2020.

[3] F. H. Giraud, S. Joshi, and J. Paik, "Haptigami: A fingertip haptic interface with vibrotactile and 3-DoF cutaneous force feedback," *IEEE Trans. Haptics*, vol. 15, no. 1, pp. 131–141, Jan.-Mar. 2021.

[4] B. MacGavin, T. Edwards, and J. L. Gorlewicz, "A protactile-inspired wearable haptic device for capturing the core functions of communication," *IEEE Trans. Haptics*, vol. 14, no. 2, pp. 279–284, Apr.-Jun. 2021.

[5] S. Follmer, D. Leithinger, A. Olwal, A. Hogge, and H. Ishii, "Inform: Dynamic physical affordances and constraints through shape and object actuation," *Uist*, vol. 13, no. 10, pp. 2501–988, 2013.

[6] J. Mullenbach, C. Shultz, A. M. Piper, M. Peshkin, and J. E. Colgate, "Surface haptic interactions with a TPad tablet," in *Proc. Adjunct Proc. 26th Annu. ACM Symp. User Interface Softw. Technol.*, 2013, pp. 7–8.

[7] A. M. Kappers and W. M. Bergmann Tiest, "Haptic perception," *Wiley Interdiscipl. Rev.: Cogn. Sci.*, vol. 4, no. 4, pp. 357–374, 2013.
[8] T. Zeng, F. Giraud, B. Lemaire-Semail, and M. Amberg, "Haptic perception of curvature through active touch," in *Proc. IEEE World Haptics Conf.*, 2011, pp. 533–538.
[9] A. M. Kappers, "Human perception of shape from touch," *Philos. Trans. Roy. Soc. B: Biol. Sci.*, vol. 366, no. 1581, pp. 3106–3114, 2011.
[10] S. Louw, A. M. Kappers, and J. J. Koenderink, "Haptic detection thresholds of Gaussian profiles over the whole range of spatial scales," *Exp. Brain Res.*, vol. 132, pp. 369–374, 2000.
[11] W. M. B. Tiest, L. M. A. Van Der Hoff, and A. M. Kappers, "Cutaneous and kinaesthetic perception of traversed distance," in *Proc. IEEE World Haptics Conf.*, 2011, pp. 593–597.
[12] M. Kahrimanovic, W. M. B. Tiest, and A. M. Kappers, "Haptic perception of volume and surface area of 3-D objects," *Attention, Perception, Psychophys.*, vol. 72, no. 2, pp. 517–527, 2010.
[13] C. Hatzfeld, S. Dorsch, C. Neupert, and M. Kupnik, "Influence of surgical gloves on haptic perception thresholds," *Int. J. Med. Robot. Comput. Assist. Surg.*, vol. 14, no. 1, 2018, Art. no. e1852.
[14] N. Zamani and H. Culbertson, "Effects of dental glove thickness on tactile perception through a tool," in *Proc. IEEE World Haptics Conf.*, 2019, pp. 187–192.
[15] S. C. Pont, A. M. Kappers, and J. J. Koenderink, "Haptic curvature discrimination at several regions of the hand," *Percep. Psychophys.*, vol. 59, pp. 1225–1240, 1997.
[16] Z. A. Zook, J. J. Fleck, and M. K. O'Malley, "Effect of tactile masking on multi-sensory haptic perception," *IEEE Trans. Haptics*, vol. 15, no. 1, pp. 212–221, Jan.-Mar. 2022.
[17] F. Barbagli, K. Salisbury, C. Ho, C. Spence, and H. Z. Tan, "Haptic discrimination of force direction and the influence of visual information," *ACM Trans. Appl. Percep.*, vol. 3, no. 2, pp. 125–135, 2006.
[18] M. Kahrimanovic, W. M. Bergmann Tiest, and A. M. Kappers, "Discrimination thresholds for haptic perception of volume, surface area, and weight," *Attention, Perception, Psychophys.*, vol. 73, pp. 2649–2656, 2011.
[19] J. Yang, T. Ogasa, Y. Ohta, K. Abe, and J. Wu, "Decline of human tactile angle discrimination in patients with mild cognitive impairment and Alzheimer's disease," *J. Alzheimer's Dis.*, vol. 22, no. 1, pp. 225–234, 2010.
[20] F. Mori et al., "Transcranial direct current stimulation ameliorates tactile sensory deficit in multiple sclerosis," *Brain Stimulation*, vol. 6, no. 4, pp. 654–659, 2013.
[21] F. Picconi et al., "The evaluation of tactile dysfunction in the hand in type 1 diabetes: A novel method based on haptics," *Acta Diabetologica*, vol. 59, no. 8, pp. 1073–1082, 2022.
[22] J. Park, A. J. Doxon, W. R. Provancher, D. E. Johnson, and H. Z. Tan, "Haptic edge sharpness perception with a contact location display," *IEEE Trans. Haptics*, vol. 5, no. 4, pp. 323–331, Oct.–Dec. 2012.
[23] J. Jiao et al., "Detection and discrimination thresholds for haptic gratings on electrostatic tactile displays," *IEEE Trans. Haptics*, vol. 12, no. 1, pp. 34–42, Jan.-Mar. 2019.
[24] M. W. Wijntjes, A. Sato, V. Hayward, and A. M. Kappers, "Local surface orientation dominates haptic curvature discrimination," *IEEE Trans. Haptics*, vol. 2, no. 2, pp. 94–102, Apr.-Jun. 2009.
[25] S. J. Lederman and R. L. Klatzky, "Hand movements: A window into haptic object recognition," *Cogn. Psychol.*, vol. 19, no. 3, pp. 342–368, 1987.
[26] J. Voisin, G. Benoit, and C. E. Chapman, "Haptic discrimination of object shape in humans: Two-dimensional angle discrimination," *Exp. Brain Res.*, vol. 145, pp. 239–250, 2002.
[27] A. M. Fernandes and P. B. Albuquerque, "Tactual perception: A review of experimental variables and procedures," *Cogn. Process.*, vol. 13, pp. 285–301, 2012.
[28] J. Wu, J. Yang, and T. Ogasa, "Raised-angle discrimination under passive finger movement," *Perception*, vol. 39, no. 7, pp. 993–1006, 2010.
[29] A. L. Skinner, C. Kent, J. M. Rossiter, C. P. Benton, M. G. Groen, and J. M. Noyes, "On the edge: Haptic discrimination of edge sharpness," *PLoS One*, vol. 8, no. 9, 2013, Art. no. e73283.
[30] C. Kent, A. L. Skinner, C. Weeds, and C. P. Benton, "Proximal-distal, not medial-lateral, movement across an edge increases discrimination of edge sharpness," *Perception*, vol. 43, no. 10, pp. 1097–1106, 2014.
[31] A. H. Holway and C. C. Pratt, "The Weber ratio for intensive discrimination," *Psychol. Rev.*, vol. 43, no. 4, 1936, Art. no. 322.
[32] C. Dhong et al., "Role of indentation depth and contact area on human perception of softness for haptic interfaces," *Sci. Adv.*, vol. 5, no. 8, 2019, Art. no. eaaw8845.
[33] A. Goodwin and H. Wheat, "Human tactile discrimination of curvature when contact area with the skin remains constant," *Exp. Brain Res.*, vol. 88, pp. 447–450, 1992.
[34] R. Ulrich and J. Miller, "Threshold estimation in two-alternative forced-choice (2AFC) tasks: The Spearman-Kärber method," *Percep. Psychophys.*, vol. 66, no. 3, pp. 517–533, 2004.
[35] B. J. Ransil and S. C. Schachter, "Test-retest reliability of the edinburgh handedness inventory and global handedness preference measurements, and their correlation," *Perceptual Motor Skills*, vol. 79, no. 3, pp. 1355–1372, 1994.
[36] Z. Zhang et al., "Discrimination threshold for haptic volume perception of fingers and phalanges," *Attention, Perception, Psychophys.*, vol. 80, pp. 576–585, 2018.
[37] IBM, "SPSS statistics - curve estimation models," 2023. [Online]. Available: https://www.ibm.com/docs/en/spss-statistics/saas?topic=estimation-curve-models
[38] D. Algom, "The Weber–Fechner law: A misnomer that persists but that should go away," *Psychol. Rev.*, vol. 128, no. 4, 2021, Art. no. 757.
[39] S. Bochereau, B. Dzidek, M. Adams, and V. Hayward, "Characterizing and imaging gross and real finger contacts under dynamic loading," *IEEE Trans. Haptics*, vol. 10, no. 4, pp. 456–465, Oct.-Dec. 2017.
[40] S. C. Hauser and G. J. Gerling, "Measuring tactile cues at the fingerpad for object compliances harder and softer than the skin," in *Proc. IEEE Haptics Symp.*, 2016, pp. 247–252.
[41] A. Goodwin, K. John, and A. Marceglia, "Tactile discrimination of curvature by humans using only cutaneous information from the fingerpads," *Exp. Brain Res.*, vol. 86, pp. 663–672, 1991.
[42] K. Johnson, "Neural basis of haptic perception," in *Stevens' Handbook of Experimental Psychology*. Hoboken, NJ, USA: Wiley, 2002, pp. 537–580.
[43] K. S. Hale and K. M. Stanney, "Deriving haptic design guidelines from human physiological, psychophysical, and neurological foundations," *IEEE Comput. Graph. Appl.*, vol. 24, no. 2, pp. 33–39, Mar.-Apr. 2004.

Qian Wu received the B.S. and M.S. degrees in engineering from the Harbin Institute of Technology, Harbin, China, where he is currently working toward the Ph.D. degree. His research interests include haptic mechanisms, wearable haptic devices, and human-computer interaction.

Jianguang Li received the B.S. and Ph.D. degrees in mechanical engineering from the Harbin Institute of Technology, Harbin, China, in 1992 and 1997, respectively. He is currently a Professor of the School of Meachatronics Engineering, Harbin Institute of Technology. His research interests include digial manufacturing and application, industrial design, and modelling and simulation in machining process.